ACS APPLIED MATERIALS & INTERFACES

Research Article

www.acsami.org

Thermoset-Cross-Linked Lignocellulose: A Moldable Plant Biomass

Sriharsha Karumuri,[†,‡] Salim Hiziroglu,[§] and A. Kaan Kalkan*[,†,‡]

[†]Functional Nanomaterials Laboratory, [‡]Department of Mechanical Engineering, and [§]Department of Natural Resource Ecology and Management, Oklahoma State University, Stillwater, Oklahoma 74078, United States

ABSTRACT: The present work demonstrates a high biomass content (i.e., up to 90% by weight) and moldable material by controlled covalent cross-linking of lignocellulosic particles by a thermoset through epoxide−hydroxyl reactions. As an example for lignocellulosic biomass, Eastern redcedar was employed. Using scanning fluorescence microscopy and vibrational spectroscopy, macroscopic to molecular scale interactions of the thermoset with the lignocellulose have been revealed. Impregnation of the polymer resin into the biomass cellular network by capillary action as well as applied pressure results in a self-organizing structure in the form of thermoset microrods in a matrix of lignocellulose. We also infer permeation of the thermoset into the cell walls from the reaction of epoxides with the hydroxyls of the lignin. Compression tests reveal, at 30% thermoset content, thermoset-cross-linked lignocellulose has superior mechanical properties over a commercial wood plastic composite while comparable stiffness and strength to bulk epoxy and wood, respectively. The failure mechanism is understood to be crack propagation along the particle−thermoset interface and/or interparticle thermoset network.

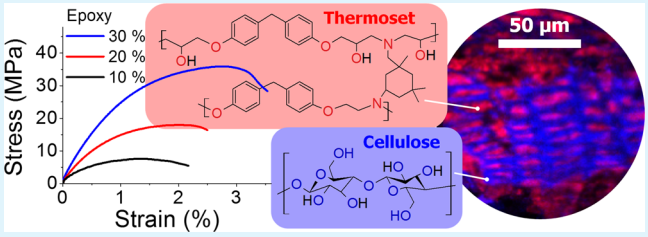

KEYWORDS: *lignocellulose, biomass, thermoset, hydroxyl, epoxide, moldable*

1. INTRODUCTION

From stover to wood, lignocellulosic biomass is characterized by cellular structures, comprised of three types of biopolymers, cellulose, hemicellulose, and lignin.[1−3] Typically, lignocellulose is made up of crystalline cellulose microfibrils embedded in aromatic biopolymer lignin matrix connected through hemicellulose. Because of this unique structural arrangement of lignocellulose, the cell wall has an elastic modulus of up to 35 GPa and yield strength of 350 MPa accounting for superior stiffness and strength.[4] However, other than lumber grade wood, utilization of lignocellulosic biomass is limited in structural applications because of smaller dimensions and higher porosity. Indeed, over 40 million tons of lignocellulosic biomass as agricultural or forestry waste is unutilized every year.[1] Although lignocellulosic biomass is the closest natural alternative to plastics, it cannot be molded or extruded like plastics. One way of transforming lignocellulose to bulk-like and moldable components is blending it with plastics to obtain biocomposites (BCs). BCs can be molded/extruded above the glass transition temperature of the thermoplastic matrix. Alternatively, olefins can be first impregnated into the cellular structure in liquid form and then polymerized for achieving a dense solid.[5] The most common form of BCs is wood plastic composites (WPCs), which combine the mechanical strength of wood with the durability and resistance of plastics against environmental exposure and biological agents, such as moisture, termites, and fungi.[6−8] Nevertheless, in comparison with lignocellulose, the stiffness and strength of BCs and WPCs are still significantly poor.

This limited performance is attributable to poor wetting of biomass particles with thermoplastic polymers and absence of covalent linking at the polymer−biomass interface. As we demonstrate in this work, an effective approach to improved polymer−biomass interface is the use of a hydrophilic phenolic thermoset, which wets as well as binds covalently to the biomass. Specifically, phenolic-based epoxy thermosets can interact with lignocellulose in two ways: first, the epoxide and hydroxyl groups of epoxy resin can react with the hydroxyl groups of lignocellulose; and second, the $\pi-\pi$ attraction between phenolic groups of thermoset polymer and lignin.[9] Epoxy thermosets have gained extensive usage in dental fillings/prostheses, nanocomposites, and superglues due to simplicity, versatility, and robustness of the epoxide cross-linking chemistry.[10] Strong covalent bonds are established through reaction of epoxy groups with amine, hydroxyl, thiol, isocyanate, and carboxylic acid groups.[10,11] However, BCs with thermoset matrix have not been fully studied and realized. A previous work had to employ a significantly large epoxy matrix fraction (i.e., 50% and larger) due to poor bonding between wood and the thermoset.[12] In this case, the epoxy matrix is expected to just confine the wood particles without adhesion. Therefore, the composite body will mechanically behave like a porous structure. Also, having a larger fraction of epoxy matrix, being expensive, increases the production cost.

The present work demonstrates thermoset-lignocellulose cross-linking can be dramatically improved by delaying the competing resin−resin cross-linking in the thermoset. Our approach involves mixing of the dry biomass powder with

Received: December 15, 2014
Accepted: March 3, 2015
Published: March 3, 2015

DOI: 10.1021/am508832d
ACS Appl. Mater. Interfaces 2015, 7, 6596−6604

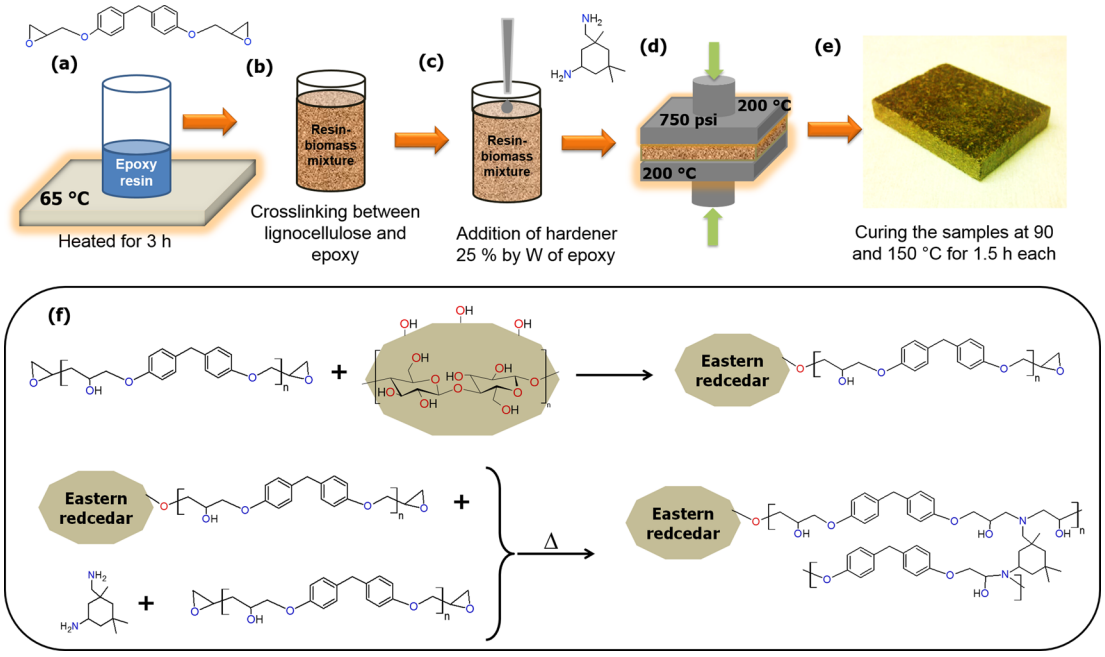

Figure 1. Schematics illustrating the procedures involved in preparation of TCL: (a) heating and degassing of epoxy resin; (b) cross-linking of resin with lignocellulose (ERC); (c) addition of hardener; (d) molding; and (e) curing. (f) Cross-linking reactions in two-stage processing of TCL. The first row illustrates the cross-linking reaction between hydroxyls in ERC and epoxides in epoxy resin, while the second row shows the cross-linking between resin oligomer chains by epoxide-amine reaction.

epoxy resin and then with curing agent in two separate stages. Because the thermoset content is as low as 5% by volume and the resin as well as curing agent is largely absorbed by the porous biomass particles, the biomass essentially remains in powder texture. However, the treated biomass powder transforms to a dough-like consistency upon compression and can be molded or extruded into any shape, that is, green body, at the ambient temperature. The final stage involves a low temperature bake to cure the green body to a solid, which hereafter is named as "thermoset-cross-linked lignocellulose" (TCL). By fluorescence microscopy and vibrational spectroscopy, we deduce the plant biomass particles are glued together by an ultrathin layer of thermoset. The thermoset matrix surrounding the particles is thin not only due to its low content but also its significant impregnation into the particles. Therefore, the role of the thermoset is covalent linking of the lignocellulose-based domains as well as enhancement of their strength/stiffness by filling the cell lumen. The plastic behavior of TCL is observed to be qualitatively similar to that of a thermoset polymer, where plateau and densification regimes of a biocellular material, such as solid wood, are absent.

In particular, the present demonstration employs Eastern redcedar (*Juniperus virginiana* L.) as the model biomass, which is an invasive species and not utilized efficiently by the lumber industry. Current area covered by Eastern redcedar (ERC) in Oklahoma is estimated as 15.6 million acres, approximately 28% of the Oklahoma landscape.[13] Although the ERC has had an instrumental role in preventing soil erosion in Oklahoma, its current population is growing at the rate of 939 acres per day, resulting in a significant adverse impact on ecology: the trees are reducing productivity from grasslands, destroying wildlife habitat, out-competing other tree species, and cause larger mortality in wildfires due to highly flammable volatile oils in the redcedar.[13] Therefore, ERC is conceived as a good example of an underutilized but renewable resource for the production of TCL in a sustainable fashion.

2. MATERIALS AND METHODS

2.1. Precursors. Di-glycidyl ether of Bisphenol F (DGEBF) resin and Isophorone Diamine (IPDA) hardener were employed in preparation of the TCL. The resin (Epon 862) and hardener (Epikure 3300) were purchased from Miller-Stephenson Inc., U.S. Prior to cross-linking, epoxy resin was heated to 65 °C on a hot plate for 3 h to eliminate bubbles and aggregates (Figure 1a). Additionally, the ERC powder was sieved on a screen to a particle size of less than 400 μm.

2.2. Material Synthesis. If conventional epoxy composite fabrication is adopted, epoxy resin, biomass, and hardener are all mixed at the same time. In this case, resin−resin cross-linking is much faster than resin−lignocellulose cross-linking. Therefore, the latter reaction cannot compete with the former, and essentially all epoxide groups are consumed by the former reaction. In the present approach, the cross-linking is controlled in two separate stages. The epoxy resin is first mixed with ERC powder using a glass rod and stored at ambient temperature for 24 h to allow cross-linking between lignocellulose hydroxyl and resin epoxide groups as illustrated in Figure 1b.

In the second stage, a stoichiometric amount of hardener is stirred into the ERC-resin mixture (Figure 1c). The resulting mixture, in powder consistency, can be molded and extruded into any shape. For proof of concept, the samples were pressed in a steel mold (110 × 110 mm^2) at a temperature of 200 °C and pressure of 750 psi (Figure 1d). Finally, the plate-shaped molded piece (Figure 1e) was cured in an oven at 90 °C for 1.5 h and then postcured at 150 °C for 1.5 h. In this report, the weight ratio of epoxy is defined as weight of resin plus curing agent, which equals that of final thermoset, divided by the total weight of resin, curing agent, and ERC.

2.3. Optical Characterization. A Nicolet iS50 FT-IR spectrometer was employed in the attenuated total reflectance (ATR) mode to evaluate the cross-linking reactions between lignocellulose and epoxy. FTIR spectra were acquired from the surface of fabricated TCLs (20% epoxy), treated ERC particles (corresponding to 20% epoxy in the TCL), and neat ERC particles at 64 scans to average and 2 cm^{-1} resolution.

DOI: 10.1021/am508832d
ACS Appl. Mater. Interfaces 2015, 7, 6596−6604

The morphology of the TCL has been investigated by scanning fluorescence microscopy (SFM) using a Leica TCS SP2 confocal microscope system equipped with Ar^+ ion (363 nm) and HeNe (543 nm) lasers. With the objective of resolving the thermoset domains in the TCL, the epoxy resin was dyed with Rhodamine B, a common fluorophore, whose excitation and emission maxima are at 554 and 627 nm, respectively. The 30% epoxy TCL samples were prepared using the dyed epoxy resin. Subsequently, they are cleaved and polished for SFM. The fluorescence images were captured from the cross-section of TCL samples by exciting the epoxy and ERC domains using a 20× objective lens.

2.4. Mechanical Testing. Mechanical properties of the TCL samples were evaluated using an Instron 5567 system in compression mode equipped with a 30 kN load cell. The compression tests were performed according to ASTM D3501-5a standard on TCL specimens of dimensions, 27 × 34 × 6 mm^3 (length (L) × width (W) × thickness (T)), with load applied along the width and at a displacement rate of 0.072 mm/min. Per ASTM D3501-5a, data were acquired and averaged from five specimens. The displacement, d, due to the compressive load, P, was obtained from the crosshead movement that was corrected for machine compliance. Further, we estimated the modulus of elasticity, E, from the obtained load versus displacement curves, using the expression, $E = ((P/WT)/(d/L))$.

3. RESULTS AND DISCUSSION

As described above, TCL is prepared in two stages due to different reactivity of epoxide groups with hydroxyls of biomass versus amine groups of curing agent.[10,11] Initially, we treat ERC particles with epoxy resin only for lignocellulose−epoxy cross-linking, which otherwise is surpassed by epoxy−epoxy cross-linking. If resin and curing agent are mixed with the ERC particles concomitantly, then the mechanical properties of the TCL samples are extremely poor, even after curing in oven. In this case, the samples can be crumbled by hand.

The cell wall of the lignocellulosic biomass has tubular geometry and consists of cellulose fibers in a matrix of lignin and hemicellulose.[3] The cellulose polymer chains in the fibers are linked together by H-bonds and oriented perpendicular to the fiber axis.[14] While the lignin content is low at the surface of the cell wall, less than 15% by weight, it increases radially toward the middle lamella layer of the cell wall up to 70%.[15] We conjecture the hydroxyl groups sticking out of the surface of the cell wall are the cross-linking sites with the thermoset. Accordingly, formation of ether and additional hydroxyl groups during cross-linking is anticipated as shown in Figure 1f. The second stage of our TCL processing involves addition of hardener for epoxide−epoxide cross-linking in the resin.

Unlike in the present work, a catalyst or temperature in excess of 200 °C is generally employed to increase the rate of epoxide−hydroxyl reaction. For example, according to Shechter and Wynstra, the hydroxyl(alcohol)−epoxide(glycidyl ether) reaction is sluggish, and heat activation is required for an observable reaction rate.[16] The purpose of employing a catalyst such as strong base or higher temperature (~200 °C) in this reaction is simply to increase the rate of alkoxide ion formation from alcohol (hydroxyl groups). Consequently, these alkoxide ions react with epoxide groups producing additional alkoxide ions. These generated alkoxide ions in turn participate in the reaction with epoxide that resembles an autocatalytic reaction.[16]

On the other hand, at 25 °C and without a base catalyst, the rate of generation of alkoxide ions is too low that epoxide−hydroxyl reaction is not observable even for days. One then may question how epoxy resin and lignocellulose can react at ambient temperature and without a catalyst in the present work. Unlike typical alcohol hardeners, pure cellulose is mildly acidic, and its acidity further increases in a biomass due to impurities.[17] This higher acidity of biomass increases the alkoxide ion generation as compared to that with conventional alcohol hardeners. Henceforth, the creation of alkoxide ions at 25 °C in cellulose and lignin of lignocellulose particles is self-catalytic in hydroxyl−epoxide reaction of resin and biomass.

Therefore, albeit not rapid, the reaction between hydroxyl and epoxide groups can take place at the lignocellulose−resin interface at room temperature and without a catalyst. Because of its slow rate, we allow this cross-linking reaction between lignocellulose and epoxy resin for 24 h. The reaction is likely limited to the interface of lignocellulose and resin, as the generation of additional alkoxide ions from hydroxyl−epoxide reaction is inhibited in the bulk due to low acidity of the resin. Additionally, the long reaction time enables resin to penetrate into biomass. Because we have not employed any solvent to ease the penetration of resin into porous structure of biomass, it requires longer time for the viscous resin to infuse into biomass. Because only epoxides at the resin−lignocellulose interface are consumed in the hydroxyl−epoxide reaction, the unreacted epoxides in the bulk are left for the resin−resin cross-linking. This second reaction is simply the conventional epoxy curing conducted at higher temperature, which cross-links resin chains by epoxide−amine reaction in the presence of an amine hardener. In result, the two distinct cross-linking reactions, (i) resin−lignocellulose (only at the interfaces) and (ii) resin−resin (in the interparticle and intraparticle domains), occur in subsequent stages and account for covalent binding of lignocellulose particles by the thermoset (lignocellulose−resin−resin···resin−resin−lignocellulose).

3.1. FTIR Spectroscopy. With the objective of corroborating our claim about cross-linking reactions between epoxy and lignocellulose, FTIR spectroscopy was employed. Figure 2a and b shows the IR absorbance spectra of ERC, epoxy resin, epoxy resin+ERC particles (after 0 and 24 h of interaction), TCL (cleaved surface), and cured epoxy. The assignments for the peaks are listed in Table 1. The spectra in Figure 2 are normalized with respect to the 1507 cm^{-1} peak (i.e., associated with C═C stretching in phenyl groups of epoxy[18]) with an exception for the spectrum of the ERC particles.

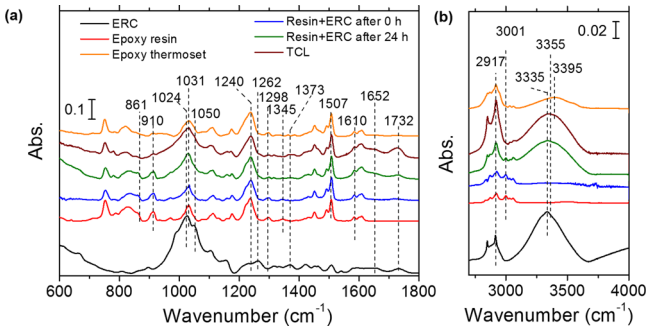

Figure 2. FTIR spectra representative of ERC particles, epoxy resin, epoxy thermoset, resin+ERC (corresponding to 20% thermoset epoxy in the TCL, after 0 and 24 h interaction), and TCL (20% epoxy) that validate the cross-linking reactions between epoxy and ERC domains for the wavenumber ranges of 600−1800 cm^{-1} (a) and 2700−4000 cm^{-1} (b).

3.1.1. Penetration of Epoxy Resin (Stage 1) into Biomass Particles. The peaks at 1652 and 1732 cm^{-1} in the lignocellulose (ERC) spectrum of Figure 2a are assigned to

DOI: 10.1021/am508832d
ACS Appl. Mater. Interfaces 2015, 7, 6596−6604

Table 1. Vibrational Modes for IR Absorbance Peaks of ERC and Epoxy Resin/Thermoset[18−21,23−31]

IR band position (cm^{-1})	assignment
3390	stretching of O−H in hydroxyl groups of epoxy[18]
3355	stretching of O−H in hydroxyl groups of TCL
3335	stretching of O−H in hydroxyl groups of ERC particles[19−21,23−26]
3001	symmetric stretching of C−H in epoxide groups of epoxy resin[18,29,30]
2918	stretching of C−H in methylene groups of ERC, epoxy, and TCL[19−21,30]
1732	stretching of C═O in aliphatic ketone/aldehyde groups of lignin[19−21]
1610 and 1507	stretching of C═C in phenyl group of epoxy and lignin[18−21]
1373	symmetric deformation of C−H in cellulose[19,20]
1345	deformation of C−H in epoxide group of epoxy resin[18]
1298	skeletal C−C vibration in epoxide group of epoxy resin[18]
1262	stretching of C−O in phenol group of lignin[19,20,27]
1240	stretching of C−O in phenoxy groups of epoxy[18]
1050	stretching of C−O in ether groups of cellulose/hemicellulose[19−21]
1031	symmetric stretching of C−O in ether groups of epoxy[18]
1024	symmetric stretching of C−O groups in primary alcohol of cellulose and lignin[19−21]
910	in-plane asymmetric deformation of epoxide ring in epoxy resin[31]
861	in-plane symmetric deformation of epoxide ring in epoxy resin[31]

C═O stretching in conjugated and unconjugated carbonyl groups of lignin, respectively.[19−21] The carbonyl groups in lignin remain unreacted during cross-linking reaction of epoxy resin and lignocellulose. Hence, the intensity of the 1652 and 1732 cm^{-1} peaks is expected to be constant during treatment of ERC with epoxy resin. In contrast, the intensity increases significantly from 0 to 24 h of treatment as observed in Figure 2a. This situation can be explained as a measurement artifact due to resin layers capping ERC particles. When the thickness of resin is 2 μm or larger, the transmission of IR radiation into/from the lignocellulose is blocked at the sensitivity level of the ATR-FTIR system used.[22] On the other hand, during interaction of resin and ERC, the epoxy gradually impregnates into biomass through pores by capillary action, and the thickness of the resin surrounding the particles decreases. Thereby, IR signal from lignocellulose (ERC) is eventually recovered.

3.1.2. Monitoring of Epoxide−Hydroxyl Reaction (Stage 1) with O−H Marker in Cellulose. The vibrational stretching of O−H associated with hydroxyl groups in cellulose is characterized by the 3335 cm^{-1} peak in the ERC spectrum (black curve in Figure 2b).[19−21,23−26] After 24 h of treatment of the ERC with resin, this peak weakens as compared to that in neat ERC, indicative of reduction of O−H concentration in cellulose. One may doubt this weakening in intensity results from attenuation of the IR signal by the residual resin on the surface of the biomass. However, when the 1732 cm^{-1} peak is adopted as the control (i.e., for normalization of the 3335 cm^{-1} peak intensity), the same conclusion persists. Therefore, reaction of O−H groups with epoxide groups is inferred. In this cross-linking reaction, first the H-bonds (−OH···O−) holding cellulose chains together on the cell wall are cleaved. Subsequently, the released hydroxyl groups undergo cross-linking with the epoxy resin. This cross-linking reaction also disrupts the crystalline arrangement between cellulose polymer chains leading to weakening in the remainder of the H-bonds. As a result, affinity of H to O in the remaining −OH groups is increased accounting for higher O−H bond stiffness as corroborated by the frequency shift from 3335 to 3355 cm^{-1}. Moreover, the new hydroxyls formed during cross-linking reactions and unreacted hydroxyls of cellulose are considered to be responsible for the observed heterogeneous broadening of the peak.

3.1.3. Monitoring of Epoxide−Hydroxyl Reaction (Stage 1) with C−O−C Marker in Lignocellulose. Next, we would like to disclose further evidence showing cross-linking of lignocellulose with epoxy. The peak at 1024 cm^{-1} in the lignocellulose (ERC) spectrum of Figure 2a is ascribed to C−O−C symmetric stretching in alcohol groups of cellulose,[19−21,23] while the peak at 1031 cm^{-1} in the epoxy resin and cured epoxy spectra is associated with the C−O−C symmetric stretching in phenyl ether groups of epoxy chains.[18] Upon interaction of resin with ERC, a decrease in the intensity of the 1024 cm^{-1} peak is seen initially at 0 h of treatment. An increase then is observed from 0 to 24 h of interaction. The initial intensity decrease is due to blocking of IR signal of ERC particles by epoxy resin encapsulation as described above. After 24 h of treatment, the signal is recovered due to thinning of resin encapsulation after its impregnation into ERC. However, the intensity of the 1024 cm^{-1} peak after 24 h is still lower as compared to the neat ERC (when normalized with respect to peak at 1732 cm^{-1}). This intensity decrease can be attributed to reduction in the concentration of alcohol groups of lignocellulose during the reaction between hydroxyl and epoxide groups.

Subsequently, we corroborate cross-linking reaction of epoxy resin with lignin. The peak at 1262 cm^{-1} in ERC spectrum in Figure 2a is ascribed to C−O stretching of phenols in lignin.[19,20,27] Once biomass is mixed with epoxy resin, we observe disappearance of this peak in the resin+ERC spectrum (at 0 h of treatment) that we attribute to capping of the ERC particles by resin. However, the peak intensity is not recovered in the resin+ERC spectrum after 24 h of incubation (i.e., despite impregnation of resin into biomass). Thereby, we infer that the concentration of C−O groups is reduced due to reaction of phenols in lignin with epoxide groups. In this reaction, the O−H moieties of phenolic groups in lignin react with epoxide groups generating phenyl ether (C−O−C) cross-links (similar to that shown in Figure 1f). The transformation of phenols in lignin to phenyl ether cross-links is further corroborated by fractional increase in the integrated area of peak at 1240 cm^{-1} of resin+ERC spectrum (i.e., C−O stretching of intrinsic phenyl ether groups in epoxy resin[18]).

3.1.4. Monitoring of Epoxide−Hydroxyl Reaction (Stage 1) with Epoxide Marker in Resin. So far, we have corroborated cross-linking of O−H groups in lignocellulose in the presence of epoxy resin, but it is not established yet if cross-linking is with the epoxides of the resin. To purport the participation of epoxide groups in this cross-linking reaction, we have investigated the vibrational peaks, which characterize the epoxide groups. The peak at 1345 cm^{-1} in the epoxy resin spectrum of Figure 2a is assigned to C−H deformation in epoxide groups of resin.[28] Meanwhile, the peak at 3001 cm^{-1} in epoxy resin spectrum of Figure 2b is associated with C−H symmetric stretching in epoxide groups.[18,29,30] It is apparent from resin+ERC spectra that these peaks have weakened during 24 h of resin−ERC interaction. In particular, the 1345 cm^{-1} peak has decreased by 2.5 ± 1.3% (computed for three sets of

DOI: 10.1021/am508832d
ACS Appl. Mater. Interfaces 2015, 7, 6596−6604

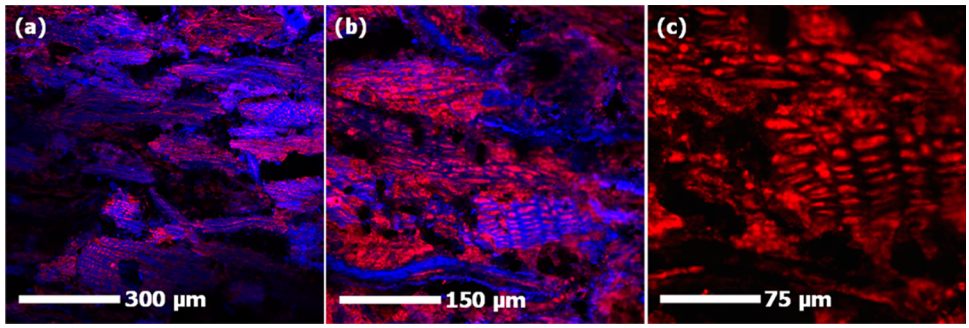

Figure 3. Fluorescence micrographs obtained by overlay of emissions from epoxy (stained with Rhodamine B) and ERC domains (a,b) for a 30% epoxy TCL sample. Magnified fluorescence micrograph showing the molded epoxy domains inside cells (c). The applied force in the molding/pressing stage is in the vertical direction with respect to the micrographs. Hence, elongation of ERC particles and cells occurs effectively in the perpendicular direction (horizontal).

data). This reduction in the peak intensities indicates a decrease of epoxide concentration due to cross-linking reaction with O−H groups. In the final processing stage, we observe the disappearance of the 1345 and 3001 cm^{-1} peaks in the TCL spectrum (i.e., after curing). This disappearance of the peaks indicates exhaustion of the remaining epoxide groups in the resin during the curing stage. The remaining epoxide groups basically react with N−H groups of hardener as well as O−H groups of lignocellulose or cured epoxy.

3.1.5. Monitoring of Epoxide−Amine Reaction (Stage 2). The peaks at 861 and 910 cm^{-1} in epoxy resin spectrum of Figure 2a are assigned to in-plane symmetric and asymmetric deformations in epoxide ring of the resin, respectively.[31] The intensity of these peaks dramatically decreases during the second stage of our TCL process. This disappearance of the 861 and 910 cm^{-1} peaks in the second stage indicates cross-linking reaction of unreacted epoxide groups. During this stage, the unreacted epoxide groups in bulk resin react with N−H groups of the hardener. The unreacted epoxide groups also react with the remaining O−H groups either in ERC or generated in epoxide−hydroxyl reaction.[11,16] As aforementioned, the simultaneous weakening of the 1024, 1262, and 3350 cm^{-1} peaks indicates diminishing of the O−H groups.

The peak at 1298 cm^{-1} in the epoxy resin spectrum of Figure 2a is ascribed to C−C skeletal vibrations in the epoxy chain.[18] We observe weakening of this peak in the TCL spectrum when normalized with respect to the 1507 cm^{-1} peak (i.e., stretching of C═C in phenyl group of epoxy). The decrease in the intensity of 1298 cm^{-1} peak is likely due to steric constraints in the C−C skeletal vibration.

The peak at 2918 cm^{-1} in epoxy resin and ERC spectra of Figure 2b is associated with stretching of C−H in methylene groups in ERC and epoxy.[19−21,30] Meanwhile, the symmetric deformation of C−H in cellulose is characterized by the peak at 1373 cm^{-1} in the ERC spectrum (Figure 2a).[19,20] The intensity of the 2918 cm^{-1} peak in the resin+ERC spectrum right after mixing (0 h in Figure 2b) is less than that in the ERC spectrum due to a lower concentration of methylene groups in epoxy resin, which is capped around ERC. In other words, the 2918 cm^{-1} peak is majorly contributed by ERC. Similarly, we notice disappearance of the 1373 cm^{-1} peak in the resin+ERC spectrum upon mixing (after 0 h) due to blocking of IR transmission by the resin. After 24 h of treatment, the intensity of the peaks has increased due to impregnation of resin, as discussed for other ERC peaks above. Moreover, we notice further increase in the intensity of peaks in the TCL spectrum. We speculate this additional enhancement in the intensity occurs because of further impregnation of residual epoxy resin by applied pressure during hot pressing.

The peaks at 1650 and 1732 cm^{-1} in the ERC spectrum of Figure 2a are ascribed to C═O stretching modes of amide and unsaturated carbonyls in lignin, respectively.[19−21] We notice an increase in the intensity of these peaks during treatment with epoxy between 0 and 24 h spectra, which is again attributed to impregnation of the resin into ERC particles. We also observe an additional increase in the intensity of these peaks after thermal curing. One may expect this enhancement in the signal is also due to further impregnation of resin into ERC particles during the molding step as described above. However, the enhancement in the intensity of these peaks (1650 and 1732 cm^{-1}) due to impregnation of epoxy during hot pressing (200 °C) is higher than that of the characteristic peaks of lignocellulose at 1373 and 2918 cm^{-1}. This additional enhancement of the 1650 and 1732 cm^{-1} peaks is attributed to increase in C═O sites as a result of oxidation at C−H moieties of cell wall components and epoxy polymer network during thermal curing.

3.2. Microstructure of TCL. The microstructure of our TCL is investigated by SFM, which allows high-resolution optical imaging due to high contrast gained between fluorescent and nonfluorescent domains. Figure 3 shows the fluorescence micrographs acquired from cleaved and polished surfaces of the TCL, which is prepared using epoxy resin stained with Rhodamine B dye. The epoxy domains in the TCL cross-section are seen in red (false color) due to Rhodamine B emission under 543 nm HeNe laser excitation, while the emissions from the ERC domains are seen in blue (false color) under excitation by Ar^+ ion laser (363 nm). Figure 3a and b shows the overlay of the two emission maps. Figure 3a clearly shows the presence of elongated ERC particles. The black domains are due to zero emission from the voids in between the particles. The majority of these voids form due to particle detachment off the surface during grinding/polishing for microscopy. As evident from the magnified micrographs of Figure 3b and c, epoxy domains are present inside the cells of the ERC particles. In general, anatomy of lignocellulose includes tracheids, pits, and vessels, which are responsible for transporting water.[3] The fluorescence micrographs show the epoxy domains are molded in such elements by impregnation of resin during the TCL processing. Unlike in natural lignocellulose, the cross-sectional view of the cellular domains (Figure 3c) shows remarkable deviation from being equiaxed.

DOI: 10.1021/am508832d
ACS Appl. Mater. Interfaces 2015, 7, 6596−6604

They are depressed in the direction of the applied molding force while elongated in the perpendicular direction. Therefore, plastic deformation of the cellular structure is inferred to occur during the molding step under applied pressure (i.e., 750 psi).

3.3. Density of TCL. This assertion about shrinking of the cellular volume (i.e., cell lumen volume) is also corroborated by the measured density of the TCL samples as given in Table 2.

Table 2. Density and Structural Parameters of the TCL Samples

epoxy content	density (g/cm^3)	epoxy volume fraction (X_e)	cell wall volume fraction (X_s)	air volume fraction (X_a)	epoxy filling ratio ($X_e/(1 - X_s)$)
0%	0.46	0	0.313	0.687	N/A
10%	1.08	0.098	0.648	0.254	0.279
20%	1.10	0.200	0.587	0.213	0.484
30%	1.12	0.305	0.523	0.172	0.640

One may perform a thought experiment and compute the theoretical maximum density of the TCL for no change in cellular volume. In this fictitious case, the interparticle volume is zero (i.e., 100% packing efficiency of the particles), and all of the epoxy is embedded into the internal cellular volume. This hypothetical case is equivalent to solid ERC, whose cellular network is partially impregnated with epoxy and for which we calculate the density as 0.52, 0.59, and 0.67 g/cm^3 for epoxy content of 10%, 20%, and 30%, respectively. Surprisingly, the actual density values in Table 2 are significantly higher. Therefore, the total cellular volume must have undergone a significant amount of reduction during the pressing/molding step. It should be remembered that the total cellular volume consists of both the impregnated epoxy and the remaining air. Another interesting result led by significant collapse of the cellular volume is the weak dependence of TCL density on the epoxy content. Despite increase of the epoxy content from 10% to 30%, the density only increases from 1.08 to 1.12 g/cm^3. This slow dependence on epoxy content underscores the fact that densification of the TCL is due to shrinking of the cellular volume for the most part, while impregnation of the epoxy into the void network plays a secondary role in densification.

Also displayed in Table 2 are volume fractions of epoxy (X_e), ERC skeleton, that is, lignocellulose (X_s), and air (X_a). These three parameters are determined by solving three equations: (i) $X_e + X_s + X_a = 1$; (ii) $d_c = d_eX_e + d_sX_s$; (iii) $(d_eX_e):(d_sX_s)$ = epoxy to ERC mass ratio. Here, d_c, d_e, and d_s are the densities of the TCL, epoxy (1.1 g/cm^3), and cell wall (average value of 1.5 g/cm^3),[4] respectively. An important figure of merit derived from these parameters is $X_e/(1 - X_s)$, the fraction of total void volume (intraparticle (cell lumen) and interparticle) filled by epoxy. We call this parameter "epoxy filling ratio", which strongly correlates with the strength of the TCL samples as discussed below.

The microstructure as represented by Figure 3 has significant implications in terms of unique properties of the TCL samples developed. During the interaction of ERC particles with epoxy resin, the liquid resin is anticipated to penetrate into tracheids and vessels by capillary action in two ways, through the cell lumen (longitudinally) and through the pits (in transverse direction), which act as gateways on the cell wall.[3] Hence, the inherent structure of plant biomass facilitates efficient impregnation of cell lumen and cell wall with epoxy resulting in a self-organizing structure in the form of thermoset microrods in a matrix of lignocellulose. As such, Figure 4 shows the improvement of mechanical properties with increasing epoxy content.

3.4. Mechanical Properties of TCL. Figure 4a depicts representative stress−strain behavior of TCL (10%, 20%, and

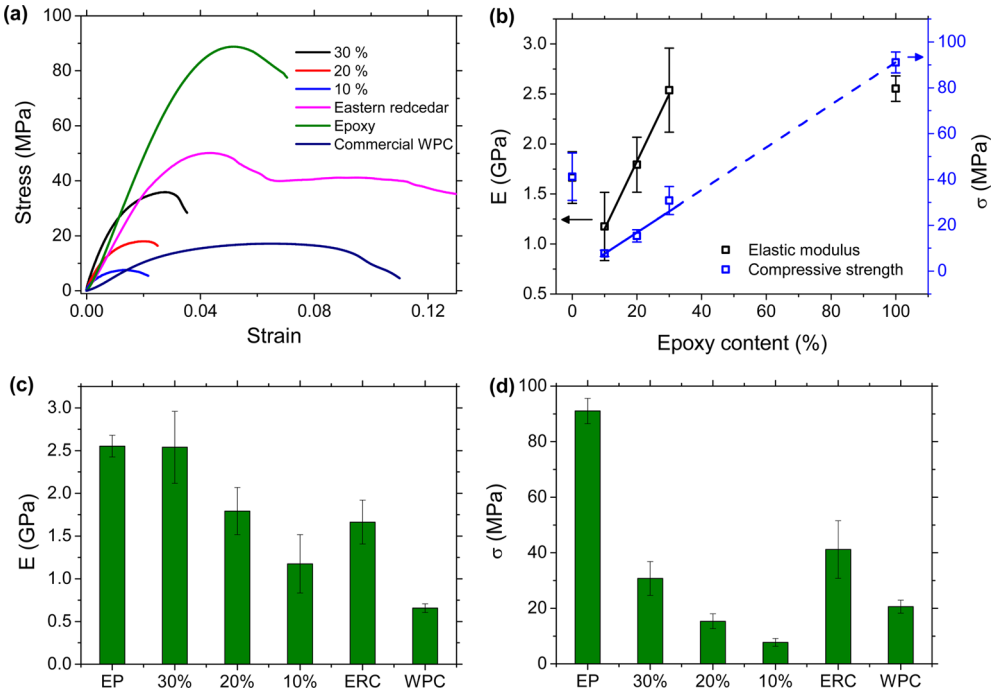

Figure 4. (a) Representative stress−strain curves of the TCL samples (10%, 20%, and 30% epoxy by weight), epoxy, bulk ERC, and commercial WPC (Trex) acquired by compression tests. (b) Increase in modulus and strength of the TCL samples with epoxy content and comparison with bulk ERC and epoxy. Comparison of the modulus (c) and strength (d) of the TCL samples with those of epoxy, bulk ERC, and commerical WPC (Trex).

DOI: 10.1021/am508832d
ACS Appl. Mater. Interfaces 2015, 7, 6596−6604

30% epoxy content), ERC, and commercial wood−plastic composite (WPC) obtained from Trex, while Figure 4b−d shows the corresponding Young's modulus and compressive strength, respectively. A typical stress−strain curve of a cellular solid such as wood, under compression, constitutes three regimes: (i) linear elastic regime associated with bending of cell walls; (ii) stress plateau (up to 70% strain) due to gradual crushing of cells by plastic yielding of cell walls; and, finally, (iii) linear regime representing densification of entire cellular structure.[32,33] However, Figure 4a shows only regimes (i) and (ii) in bulk ERC, as it undergoes failure before reaching the densification regime. On the other hand, the stress−strain curves of our TCL samples show a linear elastic regime, followed by plastic deformation with neither plateau nor densification regimes. Therefore, the stress−strain behavior also corroborates significant densification (or reduction of void volume) in our samples during processing to the degree that no further densification is measurable during the compression test. As discussed above, the densification during the TCL processing is primarily due to depression of cells when the samples are pressed for molding. The remaining cellular volume is filled by the resin.

The elastic modulus as well as compressive strength of the TCL (Figure 4b) increase with epoxy content. This improvement with the epoxy content can be owed to increased interaction of epoxy with biomass at both macroscopic and molecular levels. First, the ERC particles are cross-linked by an ultrathin epoxy layer providing structural connectivity. With increased epoxy content, a higher fraction of the particle surfaces are wetted by epoxy and cross-linked. An increase in the coverage of the epoxy layer surrounding the ERC particles is inferred with increasing epoxy content. Second, as corroborated by SFM, the void network of biomass is filled with epoxy during our TCL processing. It is anticipated that these epoxy domains act as discontinuous stiff fibers providing reinforcement to the TCL structure. These interactions led by structural coupling of the epoxy with the biomass are conveniently quantified by the epoxy filling ratio (fraction of the total void volume filled with epoxy) as given in Table 2. Third, as validated by FTIR spectroscopy, the epoxy resin reacts with cell wall components, and it is expected to increase the density and likely the strength of the cell wall.

In terms of stiffness, all of our TCL samples are superior to the commercial WPC even at 10% thermoset content. Additionally, the 20% and 30% thermoset samples exceed bulk ERC, while the 30% epoxy sample compares to bulk epoxy. The high modulus of the TCL is owed to reinforcement by stiff thermoset fibers and densification of biomass' cellular structure. High modulus also indicates efficient load transfer at the lignocellulose−thermoset interfaces validating the covalent cross-linking. The benchmark WPC sample consists of western redcedar powder and 45−50% polyethylene by weight. The higher modulus in our TCL samples is mainly due to reinforcement by the stiffer thermoset, as opposed to low stiffness polyethylene. Poor wetting of biomass particles with thermoplastic polymers and limited covalent linking also result in lower modulus and strength in commercial WPCs. In the case of TCL, the affinity between polar groups of epoxy and lignocellulosic particles allows superior wetting. This wetting followed by covalent cross-linking leads to a stronger interface.

3.5. Mode of Mechanical Failure. As observed in compression tests, the TCL samples undergo fracture after plastic deformation. The photograph of Figure 5a represents a typical sample after fracture. A magnified image of the crack is seen in Figure 5b. Release of ERC particles is also observed during the fracture. In addition, from the voids and roughness of the fracture surface, it can be deduced that the TCL samples are fractured due to rupture of the ultrathin epoxy layer at the interface between the ERC particles. Representative micrographs (bright field) of the fracture surface are given by Figure 5c−f. These photos are not easily distinguishable from their natural counterparts (i.e., as received ERC flour). The basic anatomy of the ERC particles is clearly seen including tracheids and vessels. In particular, Figure 5e and f shows the pits and perforation plates, respectively. The epoxy residues and/or epoxy-infused ERC domains are seen as darker regions.

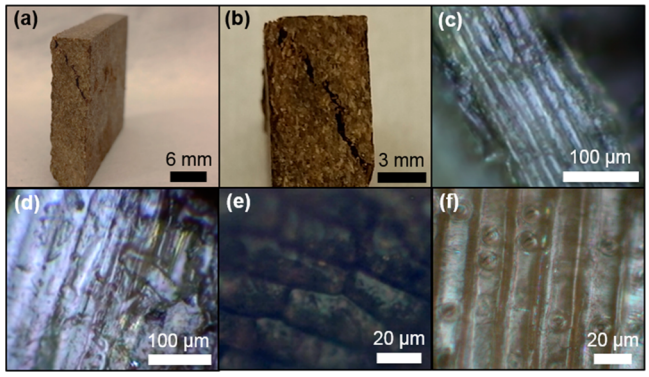

Figure 5. Photographs of a fractured TCL sample (30% epoxy) after compression test (a) and the crack in larger magnification (b). Representative bright field optical micrographs of the fractured surface (30% epoxy) showing features of ERC, fiber-tracheids (c and d), vessels and perforation plates (e), and taxodioid pits (f). The darker regions in the optical micrographs represent epoxy residues.

Hence, it is inferred that either the fracture occurs by splitting of the lignocellulose−epoxy interface, which has lower density of cross-links than the bulk epoxy, or the epoxy between the particles is weaker than bulk epoxy and this interparticle epoxy ruptures. Both cases may result from the epoxy layer covering the particles becoming too thin and discontinuous. Indeed, FTIR suggests the thickness of epoxy film capping the particles gradually decreases during the 24-h-long epoxy-ERC treatment due to flow of epoxy into the cellular volumes by capillary effects. The epoxy film may get too thin that it is not conformal around the particles, and microvoids may form in the interparticle epoxy domains leading to reduced strength. Hence, the systematic increase in strength with the epoxy content is owed to improvement of the epoxy−lignocellulose interface or interparticle epoxy domains. From Figure 4b, this enhancement is seen to be linear, and its extrapolation to 100% epoxy matches with the strength of bulk epoxy. Equivalently, the stress−strain plots of the TCL samples are qualitatively similar to those of bulk epoxy, and they are scaling up systematically with the epoxy content.

The failure mechanism being cleavage of the epoxy−lignocellulose interface or the interparticle epoxy does not imply poor cross-linking of the ERC particles, but it just reveals relatively the weakest side of the TCL. While we infer the crack propagation follows the interparticle epoxy matrix or epoxy-particle interfaces, the cell walls surrounding the brittle epoxy domains are understood to prevent crack propagation of the epoxy inside ERC particles. This phenomenon is likely due to viscoelastic nature of the cell walls allowing plastic yielding. As a result, although a crack may initiate in an epoxy domain inside

DOI: 10.1021/am508832d
ACS Appl. Mater. Interfaces 2015, 7, 6596−6604

the cell lumen, its propagation from cell to cell is impeded by the cell wall. A similar reinforcement occurs in seashells or the bone, where crack propagation from one brittle calcium phosphate/carbonate domain to another is prevented by a viscoelastic protein matrix network.[34,35] Therefore, intraparticle crack propagation does not occur. Because the crack propagation has to follow the particle boundaries, one would expect the crack path length is prolonged leading to enhancement in strength and ductility. On the other hand, the TCL samples developed in the present work exhibit lower strength and ductility as compared to bulk epoxy. Again, this lower strength and ductility as compared to bulk epoxy is attributed to lower density of cross-links in the interparticle regions.

4. CONCLUSIONS

The present work demonstrates a high lignocellulosic biomass content, high density, high strength, and moldable material by cross-linking lignocellulosic microparticles by a thermoset polymer. It is shown that lignocellulose−resin cross-linking could be dramatically improved by delaying the competing resin−resin cross-linking. High stiffness and strength of the TCL is not only attributed to strong covalent bonds at the lignocellulose−thermoset interfaces, but also to impregnation of the thermoset into the cellular structure of the biomass. The epoxy domains, which solidify inside the cells, act as discontinuous stiff and strong fibers providing reinforcement to the TCL structure. We also infer densification and strengthening of the cell walls through infusion of epoxy into them, which provides additional mechanical reinforcement. Further, the cell walls surrounding the brittle epoxy domains can prevent crack propagation from cell to cell due to their viscoelastic nature accounting for plastic yielding. Therefore, the fracture does not involve crack propagation through the cells, but it occurs through rupture of the interparticle epoxy domains or epoxy−lignocellulose interface. Because of the significant reduction of the cellular volume of biomass during molding under pressure and displacement of the remaining cellular volume by thermoset, the behavior of TCL under compression is also dramatically different from that of biomass or other cellular materials. The plateau and densification regimes in the stress−strain plots are absent. We understand the strength is governed by the quality of the epoxy−lignocellulose interface and/or interparticle epoxy, which is limited by the quantity of epoxy present at these domains at the end of the process. Additional treatments may be developed to ensure conformal coverage of the particles with the thermoset and achieve higher strength.

AUTHOR INFORMATION

Corresponding Author

*Tel.: (405) 744-5709. E-mail: kaan.kalkan@okstate.edu.

Notes

The authors declare no competing financial interest.

ACKNOWLEDGMENTS

We acknowledge the funding by Oklahoma State University (OSU) Technology and Business Development Program under Grant number 2014-12. We thank Professor Raman P. Singh and Salah U. Hamim of Mechanics of Advanced Materials Laboratory for their assistance in some of the compression tests. We also acknowledge the Undergraduate Teaching Laboratory of OSU Chemistry Department for FTIR acquisitions.

REFERENCES

(1) Sanderson, K. A Chewy Problem. *Nature* **2011**, *474*, S12−S14.
(2) Himmel, M. E.; Ding, S.-Y.; Johnson, D. K.; Adney, W. S.; Nimlos, M. R.; Brady, J. W.; Foust, T. D. Biomass Recalcitrance: Engineering Plants and Enzymes for Biofuels Production. *Science* **2007**, *315*, 804−807.
(3) Moon, R. J. *Nanomaterials in the Forest Products Industry*; McGraw-Hill: New York, 2008; pp 225−228.
(4) Moon, R. J.; Martini, A.; Nairn, J.; Simonsen, J.; Youngblood, J. Cellulose Nanomaterials Review: Structure, Properties and Nanocomposites. *Chem. Soc. Rev.* **2011**, *40*, 3941−3994.
(5) Trey, S. M.; Netrval, J.; Berglund, L.; Johansson, M. Electron-Beam-Initiated Polymerization of Poly(ethylene glycol)-Based Wood Impregnants. *ACS Appl. Mater. Interfaces* **2010**, *2*, 3352−3362.
(6) Klyosov, A. A. *Wood-Plastic Composites*; John Wiley & Sons, Inc.: Hoboken, NJ, 2007.
(7) Clemons, C. Wood-Plastic Composites in the United States The Interfacing of Two Industries. *For. Prod. J.* **2002**, *52*, 10−18.
(8) Faruk, O.; Matuana, L. M. Nanoclay Reinforced HDPE as a Matrix for Wood-Plastic Composites. *Compos. Sci. Technol.* **2008**, *68*, 2073−2077.
(9) Ermeydan, M. A.; Cabane, E.; Masic, A.; Koetz, J.; Burgert, I. Flavonoid Insertion into Cell Walls Improves Wood Properties. *ACS Appl. Mater. Interfaces* **2012**, *4*, 5782−5789.
(10) Boyle, M. A.; Martin, C. J.; Neuner, J. D. *Composites*; ASM International: OH, 2001; Vol. *21*.
(11) Pascault, J.-P.; Williams, R. J. J. *Epoxy Polymers: New Materials and Innovations*; Wiley-VCH Verlag: Weinheim, Germany, 2010.
(12) Dwivedi, U. K.; Chand, N. Influence of Wood Flour Loading on Tribological Behavior of Epoxy Composites. *Polym. Compos.* **2008**, *29*, 1189−1192.
(13) Hiziroglu, S.; Holcomb, R. B.; Wu, Q. L. Manufacturing Particleboard from Eastern Redcedar. *For. Prod. J.* **2002**, *52*, 72−76.
(14) Ding, S.-Y.; Himmel, M. E. The Maize Primary Cell Wall Microfibril: A New Model Derived from Direct Visualization. *J. Agric. Food Chem.* **2006**, *54*, 597−606.
(15) Gibson, L. J. The Hierarchical Structure and Mechanics of Plant Materials. *J. R. Soc. Interface* **2012**, *9*, 2749−2766.
(16) Shechter, L.; Wynstra, J. Glycidyl Ether Reactions with Alcohols, Phenols, Carboxylic Acids, and Acid Anhydrides. *Ind. Eng. Chem.* **1956**, *48*, 86−93.
(17) Heymann, E.; Rabinov, G. The Acid Nature of Cellulose. I. Equilibria between Cellulose and Salts. *J. Phys. Chem.* **1941**, *45*, 1152−1166.
(18) Mertzel, E.; Koenig, J. Application of FT-IR and NMR to epoxy resins. In *Epoxy Resins and Composites II*; Dušek, K., Ed.; Springer: Berlin, Heidelberg, 1986; Vol. *75*, pp 73−112.
(19) Pandey, K. K. A Study of Chemical Structure of Soft and Hardwood and Wood Polymers by FTIR Spectroscopy. *J. Appl. Polym. Sci.* **1999**, *71*, 1969−1975.
(20) Pandey, K. K.; Theagarajan, K. S. Analysis of Wood Surfaces and Ground Wood by Diffuse Reflectance (DRIFT) and Photoacoustic (PAS) Fourier Transform Infrared Spectroscopic Techniques. *Holz Roh- Werkst.* **1997**, *55*, 383−390.
(21) Faix, O.; Bottcher, J. H. The Influence of Particle-size and Concentration in Transmission and Diffuse Reflectance Spectroscopy of Wood. *Holz Roh- Werkst.* **1992**, *50*, 221−226.
(22) Schuttlefield, J. D.; Grassian, V. H. ATR−FTIR Spectroscopy in the Undergraduate Chemistry Laboratory. Part I: Fundamentals and Examples. *J. Chem. Educ.* **2008**, *85*, 279.
(23) Edlund, U.; Ryberg, Y. Z.; Albertsson, A.-C. Barrier Films from Renewable Forestry Waste. *Biomacromolecules* **2010**, *11*, 2532−2538.
(24) Hishikawa, Y.; Inoue, S.-i.; Magoshi, J.; Kondo, T. Novel Tool for Characterization of Noncrystalline Regions in Cellulose: A FTIR Deuteration Monitoring and Generalized Two-Dimensional Correlation Spectroscopy. *Biomacromolecules* **2005**, *6*, 2468−2473.

DOI: 10.1021/am508832d
ACS Appl. Mater. Interfaces 2015, 7, 6596−6604

(25) Zhu Ryberg, Y. Z.; Edlund, U.; Albertsson, A. C. Conceptual Approach to Renewable Barrier Film Design Based on Wood Hydrolysate. *Biomacromolecules* **2011**, *12*, 1355−1362.
(26) Brown, E. E.; Laborie, M.-P. G. Bioengineering Bacterial Cellulose/Poly(ethylene oxide) Nanocomposites. *Biomacromolecules* **2007**, *8*, 3074−3081.
(27) Heitner, C.; Dimmel, D.; Schmidt, J. A. *Lignin and Lignans: Advances in Chemistry*; Taylor & Francis: Boca Raton, FL, 2010.
(28) Stevens, G. C. Cure Kinetics of a Low Epoxide/Hydroxyl Group-Ratio Bisphenol a Epoxy Resin−Anhydride System by Infrared Absorption Spectroscopy. *J. Appl. Polym. Sci.* **1981**, *26*, 4259−4278.
(29) Rocks, J.; Rintoul, L.; Vohwinkel, F.; George, G. The Kinetics and Mechanism of Cure of an Amino-Glycidyl Epoxy Resin by a co-Anhydride as Studied by FT-Raman Spectroscopy. *Polymer* **2004**, *45*, 6799−6811.
(30) van Overbeke, E.; Devaux, J.; Legras, R.; Carter, J. T.; McGrail, P. T.; Carlier, V. Raman Spectroscopy and DSC Determination of Conversion in DDS-Cured Epoxy Resin: Application to Epoxy-Copolyethersulfone Blends. *Appl. Spectrosc.* **2001**, *55*, 540−551.
(31) Nyquist, R. A. *Interpreting Infrared, Raman, and Nuclear Magnetic Resonance Spectra.*; Academic Press: New York, 2001; Vol. *2*.
(32) Gibson, L. J. Biomechanics of Cellular Solids. *J. Biomech.* **2005**, *38*, 377−399.
(33) Gibson, L. J.; Ashby, M. F.; Harley, B. A. *Cellular Materials in Nature and Medicine*; Cambridge University Press: Cambridge, UK, 2010.
(34) Smith, B. L.; Schaffer, T. E.; Viani, M.; Thompson, J. B.; Frederick, N. A.; Kindt, J.; Belcher, A.; Stucky, G. D.; Morse, D. E.; Hansma, P. K. Molecular Mechanistic Origin of the Toughness of Natural Adhesives, Fibres and Composites. *Nature* **1999**, *399*, 761−763.
(35) Ritchie, R. O. The Conflicts between Strength and Toughness. *Nat. Mater.* **2011**, *10*, 817−822.

DOI: 10.1021/am508832d
ACS Appl. Mater. Interfaces 2015, 7, 6596−6604